PROCEEDINGS OF SPIE

Slot-vee antenna-coupled electro-optic modulator

Lee J. Burrows, William B. Bridges

SPIE.

Slot-Vee Antenna-Coupled Electro-Optic Modulator

Lee J. Burrows and William B. Bridges
California Institute of Technology

Abstract

We have demonstrated slot vee antenna-coupled electro-optic (Mach-Zehnder amplitude) modulators at 24 GHz (optical wavelength 1.3 µm). The slot vee antenna design allows for a more robust microwave signal feed into the $LiNbO_3$ chip, where the modulator itself acts as a slab waveguide for the microwave signal. The antenna-coupled design overcomes the velocity mismatch problems inherent in $LiNbO_3$ traveling-wave electro-optic modulators.

Introduction

Figure 1 is a schematic representation of a traveling-wave electro-optic modulator. An optical waveguide is formed in the surface of an electro-optic crystal, typically lithium niobate. Metal electrodes are deposited on the surface on either side of the optical waveguide (or the edge of one electrode may actually cover the waveguide). The electrodes form a transmission line with a characteristic impedance equal to that of the driving signal source. Typically, the transmission electrodes would be terminated in the same characteristic impedance (not shown). The potential advantage of using this traveling-wave structure is that the velocity of the modulating voltage wave along the transmission line can be equal to that of the optical wave through the optical waveguide. Thus the two waves travel in synchronism, and the modulator may be made as long as desired (limited only by the size of the crystal available and the r-f loss in the electrodes).
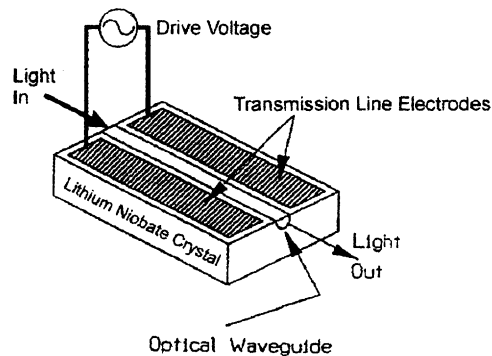
Traveling-Wave Phase Modulator

Figure 1. Schematic representation of a traveling wave phase modulator.

Unfortunately, this potential is not realized with the simple structure shown in Fig. 1 due to the inherent properties of the substrate crystal. Lithium niobate has an optical index of about 2.2, so the wave velocity in the optical waveguide is about $c/2.2$. However, it has a bulk index of about 5.6 at r-f and microwave frequencies, which results in a wave velocity along the electrodes of about $c/3.8$ to $c/4.0$ for the arrangement of planar electrodes on the surface as illustrated. (The wave moves faster than a plane wave in the bulk, $c/5.6$, because only part of the electric field between the electrodes is in the

substrate material, and part is in the air above it.) As a consequence, the modulating wave and the optical wave will eventually become out of phase as the modulator length is increased, and the modulation will actually decrease as a sinc function of the velocity mismatch, thus limiting the effective length of the modulator.

Various schemes have been used to achieve velocity matching in traveling-wave modulators and thus allow longer, more sensitive modulators to be realized. One method (e.g., Ref 1.) is to draw more of the electric field out of the substrate and into the air, usually by interposing a thick, low index buffer layer (typically silicon dioxide) between electrodes and the lithium niobate. The electrodes themselves are also electroplated so that they stick up above the substrate, also drawing the field out of the substrate. In this way, the transmission line velocity can be made equal to c/2.2, and the length of the modulator may be increased indefinitely. Of course, drawing the fields out of the substrate also reduces the overlap integral of these fields with the optical waveguide, thus reducing the magnitude of the modulation for a given applied voltage. The intent of this scheme is that the extra length will more than make up for the loss in sensitivity, especially for mm-wave modulation. In the mm-wave regime, the actual effective length of the modulator may be limited by the transmission line loss, which increases exponentially along the line.

Another scheme used (e.g., Ref. 2) is that of periodically transposing the transmission line electrodes, introducing a periodic phase shift of 180 degrees. As the modulating wave along the transmission line runs out of phase, it is periodically reset by 180 degrees. Of course, this only happens at the modulating frequency that produces a 180-degree phase error in traveling the distance between transpositions. It is "phase matching on the average", where the velocity mismatch is allowed to exist over a segment of the transmission line, but is then corrected at the end of that segment, so that the effective velocity from segment to segment is c/2.2. The overall modulator may then be as long as you like. There are three disadvantages with this scheme: First, the inherently low-pass modulator illustrated in Fig. 1 now becomes a band-pass modulator around a center frequency determined by the modulating frequency, the velocity mismatch and the length of the segmentation. Second, the bandwidth of the modulator response around this center frequency decreases with increasing number of segments. And third, as with the previous velocity matching scheme, the actual effective length may be limited by the exponential transmission line loss.

Antenna-Coupled Modulators

Several years ago, we introduced a different scheme (Refs 3,4) of "phase matching on the average," illustrated in Fig. 2. In this scheme, the transmission line is also broken into segments, and re-phased at the beginning of each segment. In this arrangement, each transmission line segment is fed by an antenna, integrated on the surface of the crystal (shown in Fig. 2 as simple dipoles). The linear array of antennas is illuminated at the correct angle so that the effective phase velocity of the illumination is just c/2.2 along the array. Figure 3 shows that the correct angle (in the case of lithium niobate) requires illumination from below at an angle θ of about 24 degrees from the normal to the modulator surface.

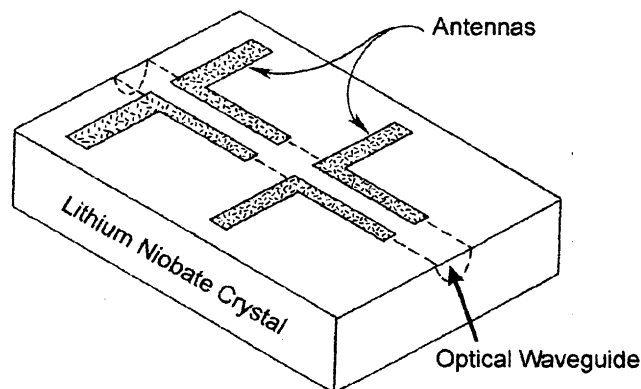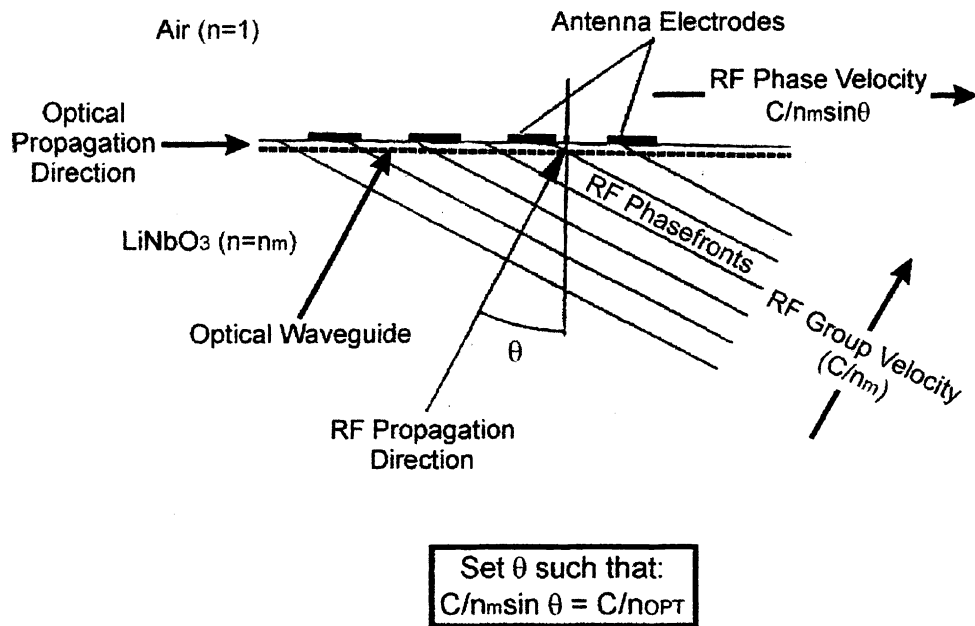Figure 2. Antenna-coupled modulator with simple dipole antennas.

57

Air (n=1)

Antenna Electrodes

RF Phase Velocity
C/n$_m$sinθ

Optical
Propagation
Direction

RF Phasefronts

LiNbO₃ (n=n$_m$)

RF Group Velocity (C/n$_m$)

Optical Waveguide

θ

RF Propagation
Direction

Set θ such that:
C/n$_m$sin θ = C/n$_{OPT}$

The antennas are located at the interface between air and
LiNbO₃. The modulating signal is incident on the antenna
array from the inside the LiNbO₃ at the angle which provides
a phase-velocity match.

Figure 3. Illumination of the dipole array from below,
at the proper angle for velocity matching.

Modulators using this "antenna-coupled" method have been demonstrated at 10, 60, and 94 GHz. Like the phase-reversal method, this scheme also converts the low-pass modulator into a band-pass modulator. However, unlike the phase-reversal method, the bandwidth around the center frequency is just the bandwidth of a single antenna-plus-segment, and is not decreased by using many such electrodes. Further, the exponential attenuation along a single transmission line segments is reduced by the number of segments, since each segment is driven by a fresh sample of the source wave. (Of course, the source wave is also divided by the number of segments to begin with, so whether this is a net advantage or not depends on whether $(1/N)e^{-\alpha L/N}$ is bigger or smaller than $e^{-\alpha L}$, where α is the attenuation per unit length along the electrodes, N is the number of segments, and L is the total length of the modulator.)

A typical feed arrangement for this kind of antenna-coupled modulator for use at 60 GHz is shown in Fig. 4 (Ref. 4). A tapered dielectric slab waveguide is inserted into the end of WR-15 waveguide (0.150 inches wide). This taper makes the transition up to the desired width of about 0.500 inches for the particular modulator shown (with 18 antenna-plus-segments patterns on it). A quarter-wave section of Stycast $\varepsilon = 9$ material was used to reduce the reflection from the tapered polypropylene guide into the lithium niobate slab guide. The lithium niobate slab was cut with a 23-degree wedge, so that the wave entered the bottom surface of the modulator at the correct matching angle. The modulators reported in Refs 3,4 were all of this type, and were designed and built by Finbar Sheehy as part of his doctoral work.
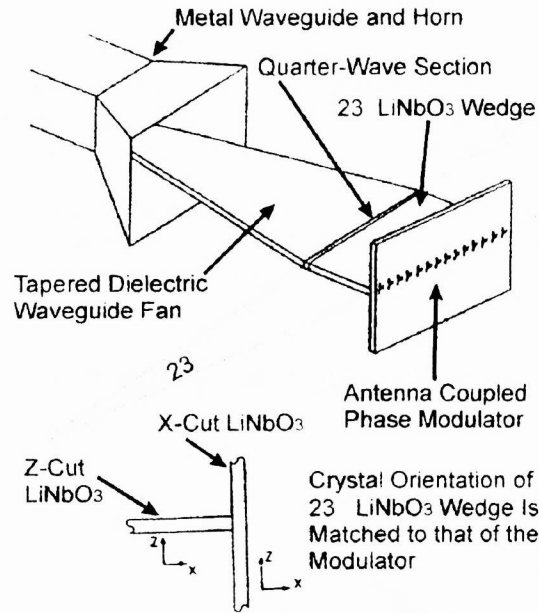
58

Figure 4. 60 GHz array of simple dipole-segment array illuminated with a tapered dielectric slab guide from a WR-15 waveguide.

Slot-Vee Antenna-Coupled Modulator Concept

Sheehy also investigated other possible integrated antennas that could be used in such a modulator (Ref. 5), particularly the class of vee antennas, with the hope of realizing some antenna gain and directivity. While the vee antennas looked promising, the complementary antenna, the "slot vee" antenna looked even more promising. The vee antennas would exhibit gain in principle, and could be designed to have the proper directivity (23 degrees off normal down into the substrate). However, the slot vee antenna has gain and directivity *parallel* to the substrate surface. The reason for this is illustrated in Fig. 5.
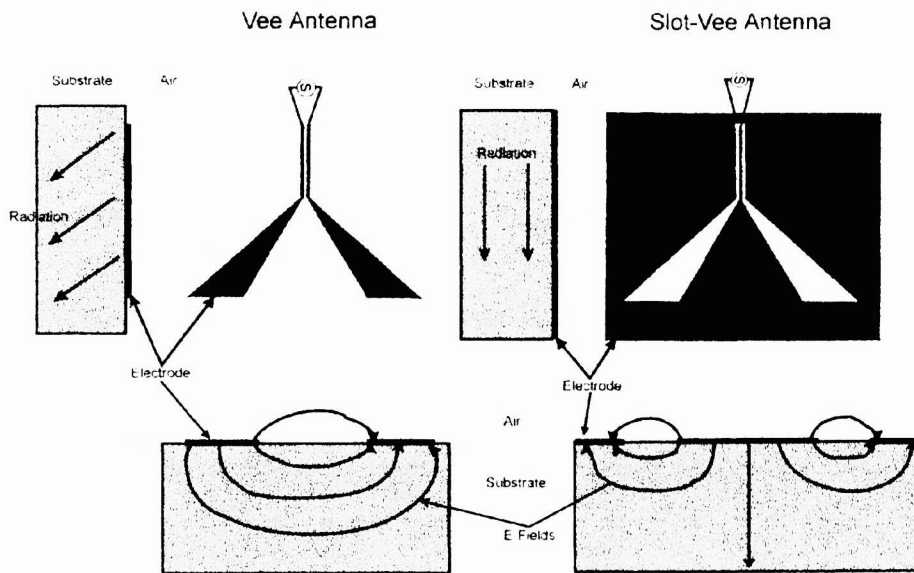
Figure 5. Comparison of vee and slot vee antennas and fields.

Booker's extension of Babinet's principle (Ref. 5.5) states that when conductor and insulator are interchanged in making the complementary antenna, the electric and magnetic fields reverse roles. Thus, the slot vee antenna is vertically polarized (i.e., the electric field is normal to the surface) while the vee antenna is horizontally polarized (parallel to the surface). Further, the fact that the dielectric-air interface is now covered by a metallic conductor removes the "null" in the direction of that interface that necessarily exists for an uncovered dielectric-air interface. The vertically polarized radiation travels under this metallic surface, and the antenna has a peak response in a direction parallel to the interface.

So then how does one introduce the required "tilt" of the illumination to perform the phase matching on the average? Sheehy's invention was to cant the antenna on the surface 23 degrees from the normal to the electrode segments, as shown in Fig. 6. And now a nice matched termination to the transmission line segment can also be made by "terminating"

20 GHz Slot-Vee Antenna Element

4000
1940
1435
1135

Optical Waveguides

$\theta=\text{arcsine}(n_m/n_{OPT})$

4025

Frequency Scaling: Dimensions Shown Here
Are For 20 GHz. To Scale for Other Frequencies,
Multiply Dimensions By 20/Freq.(GHz).

(Shaded areas represent aperture,
unshaded area represents metalization)
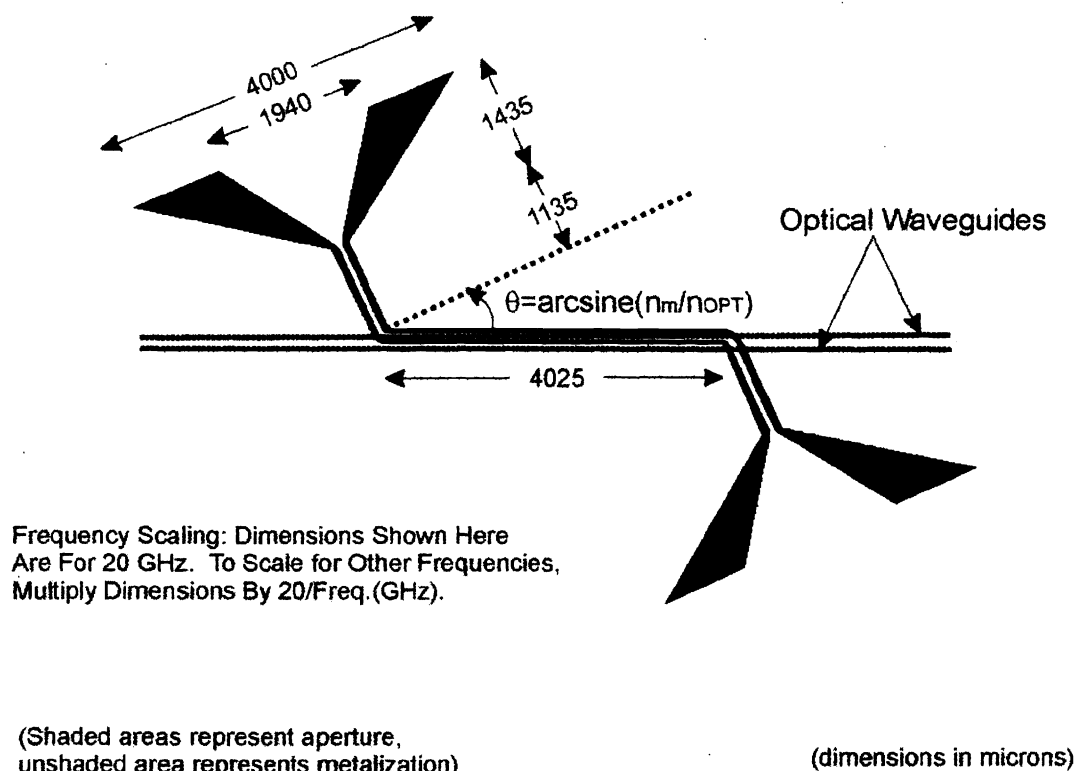
(dimensions in microns)

Figure 6. 20 GHz slot vee modulator antenna segment relative to optical waveguides.

the segment in another canted slot vee antenna connect to the far end of the segment. Thus, the signal is radiated back into the modulator slab, now being used as a dielectric waveguide as well as the modulator substrate. The overall modulator, with several such segments is shown schematically in Fig. 7 and pictorially in Fig 8, both from Sheehy's thesis (Ref. 5).
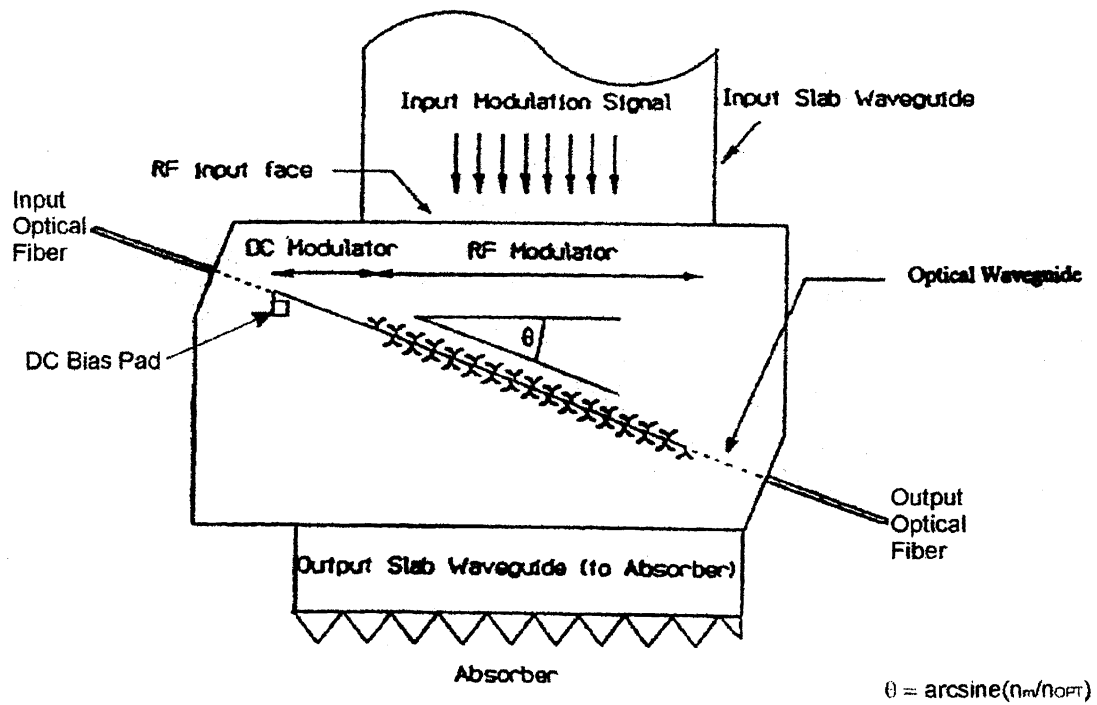
60

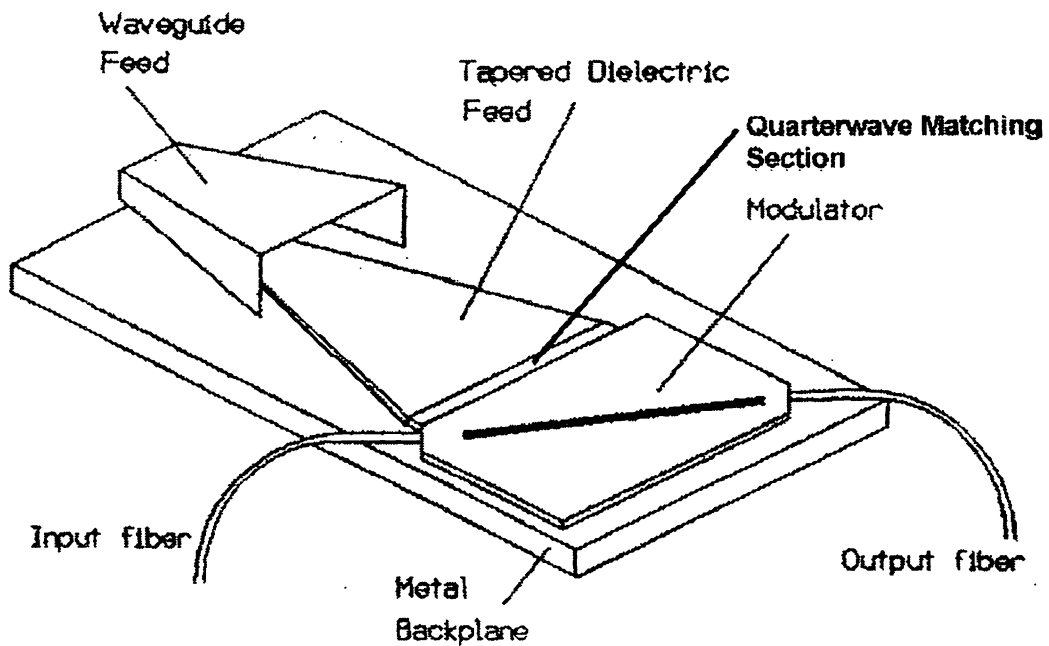Figure 7. Velocity matching with slot vee antennas.

Figure 8. Sheehy's slot vee modulator concept.

61

Slot-Vee Antenna-Coupled Modulator Experimental Results

We undertook the reduction of Sheehy's idea to practice by designing and building modulators for center frequencies of 20, 44 and 94 GHz (although we expected the operating bandwidths to be large because of the broad-band nature of the slot-vee antennas and the fact that we would have effectively terminated transmission line segments). Figure 9 shows the details of the electrode evaporation mask used to fabricate modulators at 20, 44, and 94 GHz. A negative mask is shown;
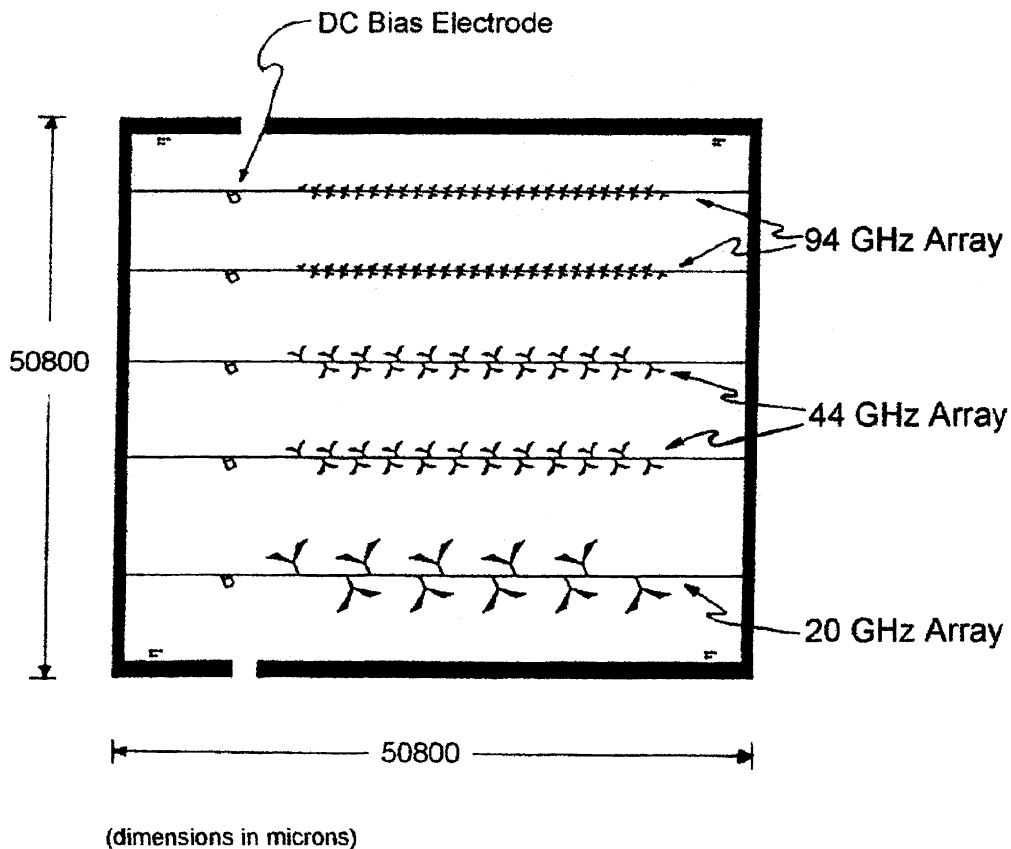

Figure 9. Slot vee modulator antenna and waveguide mask. Note the separate dc-bias sections.

the entire surface of the lithium niobate piece is covered by evaporated gold except where the slot antennas and transmission lines are shown dark in the figure. After the Ti-indiffused optical waveguides were fabricated on a 3" diameter piece of lithium niobate, SiO_2 was deposited onto the wafer, which was then cut into individual strips and a Cr-Au metallic covering was evaporated onto the surface.

The microwave feed and mechanical support for the modulator chip is shown in Fig. 10. For the 20 GHz modulator, WR-42 waveguide was used at the input, followed by a tapered height section to reduce the size of the waveguide to 0.040 inches (1mm) in height (to match the thickness of the standard lithium niobate substrate) by the standard width, 0.420 inches. The taper was followed by a uniform region of this same reduced-height cross section, in which a matching section
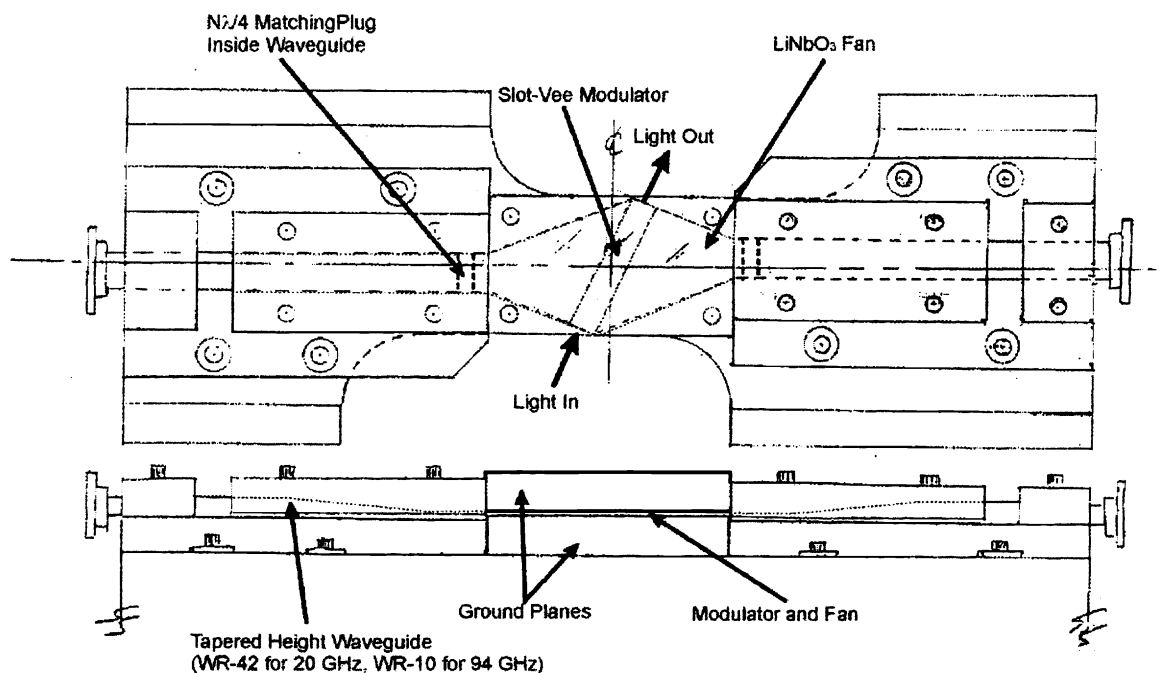
62

Figure 10. Slot vee modulator and microwave feed set-up.

of Stycast ε = 4 material was fit to fill the waveguide cross section and be five quarter-waves in length at 24 GHz. (While the original modulator had been designed for 20 GHz, the availability of a higher power microwave source at 24 GHz caused us to do the matching at that frequency.) The matching plug was followed in the reduced height section by a plug of lithium niobate, also fit to fill the guide and be flush with the end of the guide. The end of the reduced-height guide was followed by a tapered section of lithium niobate (1mm thick) which tapered up to the 3 inch length of the modulator. This lithium niobate slab was sandwiched between upper and lower metallic planes, to form a dielectric-filled parallel-plane wave guide taper.

The modulator chip was also sandwiched in this parallel plane dielectric slab guide, antenna slots down. A cavity cutout in the aluminum conductor prevented the lower plane from shorting out the fields on the "air" side of the modulator, and also allowed the attachment of the bias lead to a short dc-section of the electrodes (allowing control of the proper bias point of the Mach-Zehnder optical waveguide structure over which the electrodes were evaporated.)

A mirror image arrangement of taper, matching segments and waveguide ended in standard WR-42 waveguide, which was then terminated by a waveguide dummy load. This symmetrical arrangement allowed microwave transmission loss measurements from flange-to-flange. We then assumed that the loss from flange-to-modulator was one half the overall transmission loss, in order to obtain an estimate of the input feed loss to the modulator. This loss was measured over the frequency range of 18 to 26 GHz, and varied from 15 to 24 dB. At the primary operating frequency of 23.472 GHz, the flange-to-flange loss was 22.3 dB. We assume that the flange-to-modulator loss is one-half that value, or 11.15 dB. This may not actually be true, because of the complicated reflections that may take place in the two tapered sections of lithium niobate bounding the modulator, but it is our best guess at this point.

Modulation was detected by measuring the sideband-to-carrier ratio on a scanning Fabry-Perot display, as illustrated by the photo in Fig. 11. The modulation percentage m is given by the equation $m = 4 * \sqrt{\dfrac{P_{SIDEBAND}}{P_{CARRIER}}}$, where $P_{CARRIER}$ and $P_{SIDEBAND}$ are the measured carrier and sideband peaks on the SFP display. Note that this equation gives an

63
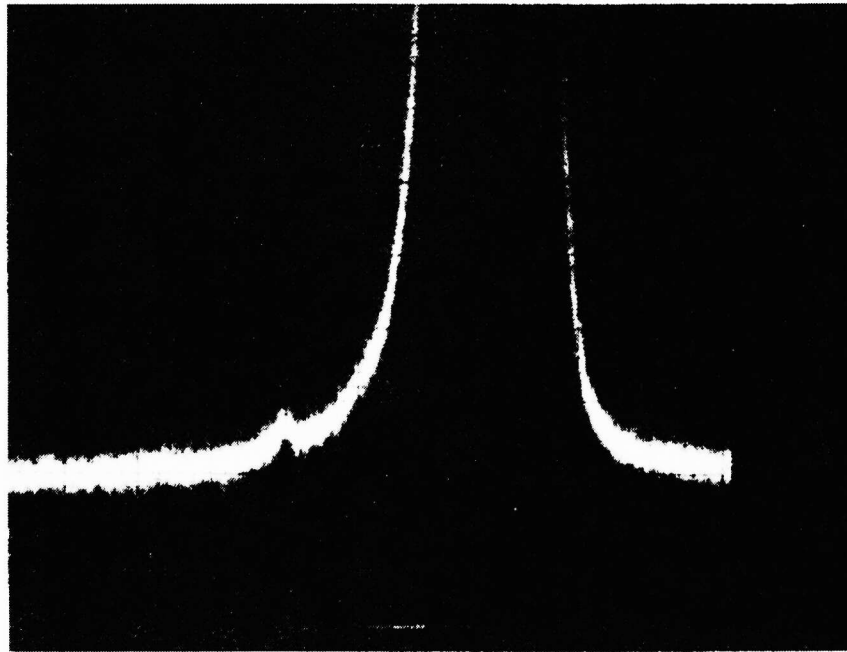
y = 5 mV/div   x = 50 MHz/div

Figure 11. Polaroid photo of scanning Fabry-Perot output showing modulation.

unambiguous value for m only if pure intensity modulation is present, as it was in this case, with a balanced electrode Mach-Zehnder arrangement. For modulators with phase modulation (for example, if only one arm of the MZ were modulated, or the two arms were not modulated equally), then the upper and lower sidebands would not be equal in amplitude. In our case, the two sidebands were of equal size.

The display in Fig. 10 is complicated by the fact that the laser used in this experiment (an ATX model 1.3-U, with 100 milliwatts at 1310 nm optical power fiber coupled into the modulator) was not running single frequency. Thus, multiple "carriers" are aliased onto the SFP display, each with their own set of upper and lower sidebands (both of which are displayed modulo 2 GHz, the free spectral range of our SFP). It likely would have been easier to detect the modulation directly with a 24 GHz photodetector, but the SFP sideband method gives a direct value without sensitivity calibration, and also works at any modulation frequency, including 44 and 94 GHz, where we planned to operate as well.

The 23.472 GHz signal was supplied by a Varian VA-98M reflex klystron, delivering 290 mW into the WR-42 flange of the waveguide set up. This results in an uncorrected figure of merit for the modulator of 0.170 m^2 / Watt, or an equivalent V_π of 76.25 Volts, assuming an active length of the modulator of 20.125 mm. Unfortunately, 2 of the 5 antenna-plus-transmission line segments were shorted, so this active length should be corrected by 3/5. And if the microwave power is corrected for the flange-to-modulator loss of 11.15 dB, then m^2 / Watt becomes 2.21 with an equivalent V_π of 21.12 Volts. The correction for loss assumes that a better job could be done in delivering the microwave signal to the vicinity of the modulator.

Another likely source of loss in this particular modulator was the connection between the evaporated coating on the surface of the modulator and the lower aluminum ground plane of the feed parallel plate line. When the section of aluminum ground plane with the cavity (used to keep from shorting out the fields in the air side of the slot vee antennas) was replaced by a continuous aluminum plane, so that the transmission did not depend on the connection or the skin-depth loss in the

64

evaporated coating, the transmission loss decreased by 7 dB. A thicker coating and better connection should yield improved performance.

A further difficulty in this experiment was encountered in the optical waveguides themselves. In the particular modulator chip evaluated here, the waveguides were not single mode at 1.3 micron wavelength. Even with the most accurate alignment, the contrast ratio of the Mach-Zehnder modulator was poor, about 2:1 at best. This had the effect of producing a large carrier feed-through that reduces the $P_{SIDEBAND} / P_{CARRIER}$ ratio. Thus, our measurement likely underestimates the actual performance this modulator would have shown in m^2 / Watt if the optical waveguides had been truly single mode.

Conclusion and Future Plans

We have demonstrated the slot-vee antenna-coupled modulator proposed by Sheehy. The performance at 24 GHz, while not competitive with standard traveling-wave electro-optic modulators, is at least promising, given the known deficiencies with the experiment. We hope to remove these deficiencies in future experiments at 44 and 94 GHz.

Acknowledgements

References

1.   G.K. Gopalakrishnan, et al, "Performance and Modeling of Broadband LiNbO$_3$ Traveling Wave Optical Intensity Modulators," J. Lightwave Tech, vol. 12, pp. 1807-18, 1994.

2.   Alferness, et al, IEEE JQE, QE-10 March 1984, pp. 301-9.

3.   Bridges, et al, "Wave-Coupled LiNbO$_3$ Electrooptic Modulator for Microwave and Millimeter Wave Modulation," IEEE Phot. Tech. Lett., vol. 3(2), pp. 133-5, 1991.

4.   Bridges, et al, "60 GHz and 94 GHz Antenna-Coupled LiNbO$_3$ Electrooptic Modulators," IEEE Phot. Tech. Lett., vol. 5(3), pp. 307-10, 1993.

5.   Sheehy, Finbar, "Antenna-Coupled mm-Wave Electro-Optic Modulators and Linearized Electro-Optic Modulators," Ph.D. Thesis, California Institute of Technology, Pasadena, CA 1993

5.5   H.G. Booker, "Slot Aerials and Their Relation to Complementary Wire Aerials," JIEE (*Lond.*), 93, pt. IIIA, no. 4, 1946.